

**Supplemental Figure 1. ChIP-seq binding profiles of individual biological replicates.** ChIP-seq enrichment scores for each replicate are shown across a representative genomic region. The corresponding GEO entries are given in Supplemental File 1. The sample nomenclature starts with the target (e.g. H3K27ac), the strain the ChIP was performed in (e.g. N2), the developmental stage (e.g. Emb), and a unique data ID for each biological replicate (e.g. LW201)

**Supplemental Figure 2. ChIP-seq ATAC-seq and DNase-seq profiles in embryo and L3 worms.** ChIP-seq binding profiles for averaged data sets across a representative region of the X. Transcriptionally inactive regions are outlined in blue and active regions in green.

**Supplemental Figure 3. Filtering DPY-27 ChIP-seq binding peaks.** DPY-27 and Pol II ChIP-seq profiles are shown along with all peaks and top 50% of peaks based on average enrichment.

**Supplemental Figure 4. Correlation of ChIP enrichment between data sets at TSS. (A)**

Spearman rank correlations of average ChIP-seq enrichment within 1 kb regions centering at the GRO-seq defined TSS sites on the X chromosome. ChIP data from *dpy-21* (CB428) and wild type (N2) embryos are plotted. Histone modifications associated with active transcription show positive correlation with RNA Pol II binding. Moreover, high correlation between wild type and mutant ChIP scores support the idea that the DCC does not drastically change the distribution of the marks, but rather tunes their level. **(B)** Spearman rank correlations between standardized log<sub>2</sub> ratios of ChIP-seq enrichment (*dpy-21*/wild type) at the 1 kb GRO-seq TSS regions across the X and autosomes. There was no strong correlation between change in RNA Pol II binding and change in histone modifications in the mutant compared to wild type. An X-specific negative correlation between DPY-27 binding and H3K27ac, supports DCC binding being linked to a reduction in H3K27ac on the X.

**Supplemental Figure 5. ChIP-seq enrichment changes in the DCC mutant and knockdown.**

**(A)** Data was analyzed as in Figure 3J and 4B, but all chromosomes are shown. DCC depletion or mutation did not significantly or specifically affect the level of H3K27me1, H3K4me1, and H3K27me2 on the X chromosomes. However, ChIP-seq data using antibodies against these modifications showed lower signal, precluding strong conclusion. **(B)** As in A, but change in histone modifications were calculated across 1 kb windows centering at Wormbase defined transcription start sites. Due to trans splicing of most genes in *C. elegans*, these TSS coordinates are less accurate, but majority fall within 500 bp of real transcription start sites (KRUESI *et al.* 2013). DCC depletion or mutation does not specifically affect H3K27me2 and H3K9me3 but leads to increased H3K27ac across these Wormbase defined transcription start sites. Boxplots are plotted as in Figure 3. \* p-value ≤ 0.001 (two-tailed Student's t-Test).

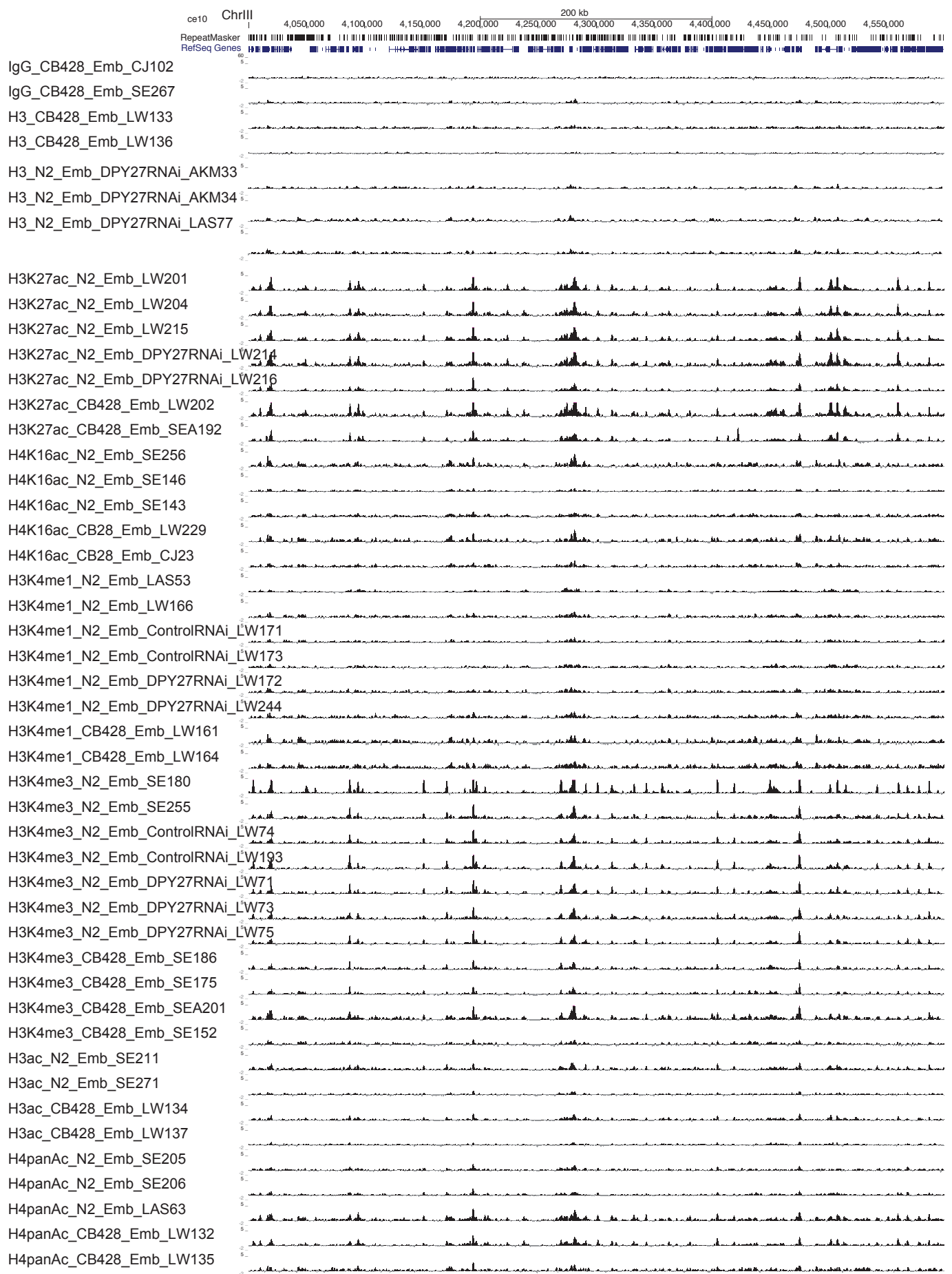
**Supplemental Figure 6. Analysis of histone modification changes in X;V fusion**

**chromosomes. (A)** Standardized log<sub>2</sub> ratios of H3K27ac enrichment within 200 bp centering at the wild type H3K27ac ChIP-seq peak summits in X;V versus wild type larvae. Individual data points within the middle, left and right most 1 Mb of each chromosome are plotted. The mean ratio for each region is shown as a line. p-values were generated from a two-tailed Student's t-Test are shown above the data. **(B)** Average DPY-27 ChIP-seq scores for 1 kb GRO-seq defined TSS regions are shown. For each 200 kb window moving along the chromosome with 20 kb steps, ChIP-seq and mRNA-seq ratios in X;V/wt were compared to the rest of the windows and a p-value

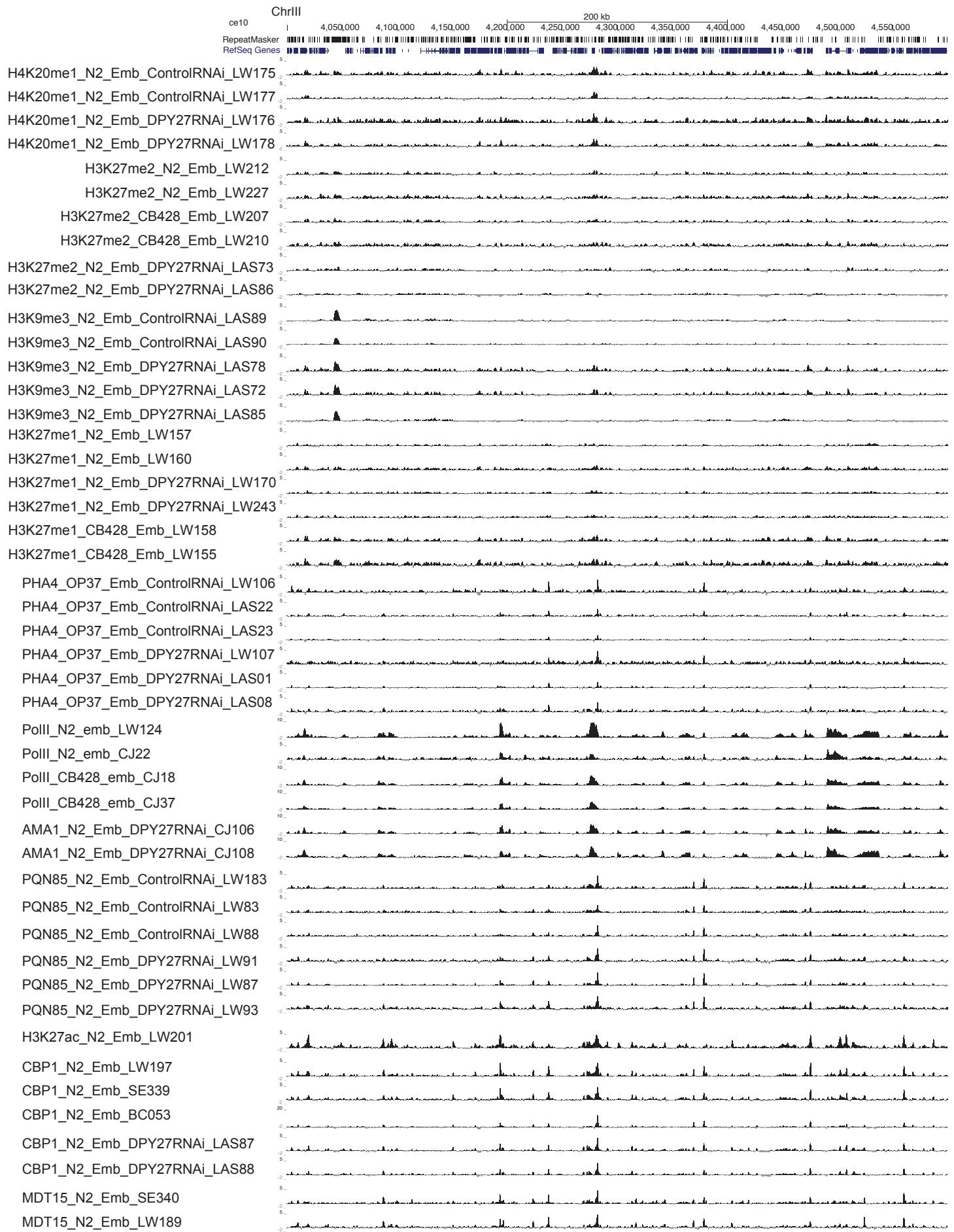
statistic was generated through t-test. Windows with  $a = p\text{-value} \leq 0.01$  are plotted. As opposed to the chromosome V, where the windows are clustered around the region of spreading (Figure 5E), on chromosome I and II, the windows containing significant changes in gene expression and histone modifications do not show noticeable clustering.

**Supplemental Figure 7. Validation of MDT-15 antibody.** modENCODE generated MDT-15 Q4097 antibody was validated by western blot analysis. In N2 wild type embryos, the antibody pulled down a protein (left panel) corresponding to a band whose intensity reduced upon *mdt-15* RNAi (compare MDT-15 signal in lane 1 to lane 4, which have similar loading based on tubulin blot). Image J was used to quantify band intensity and percentage reduction was calculated for each lane by taking a ratio of RNAi/vector MDT-15 signal versus tubulin control signal. The discrepancy between predicted MDT-15 protein size and the observed size is unclear.

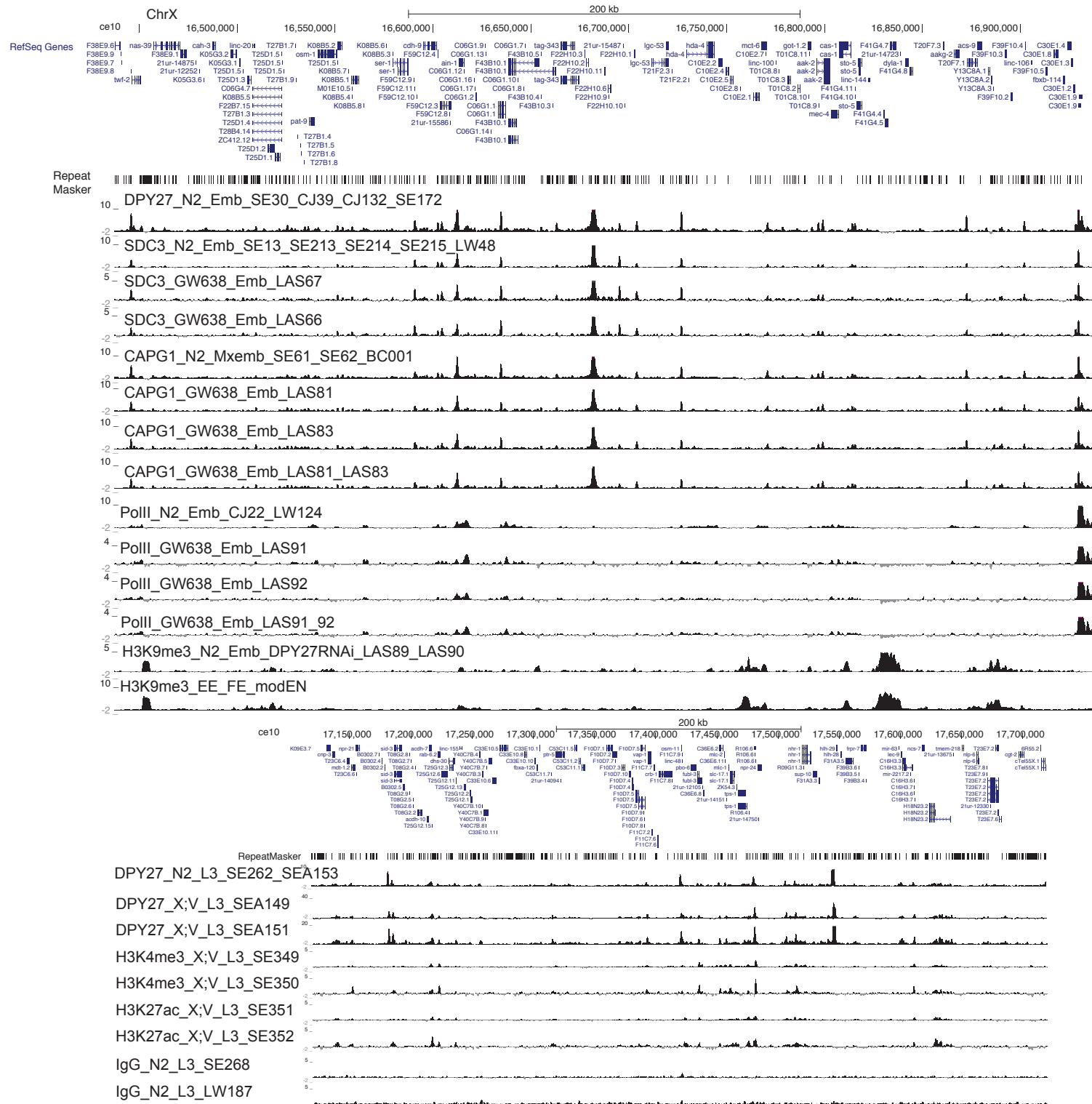
# Supp Fig 1



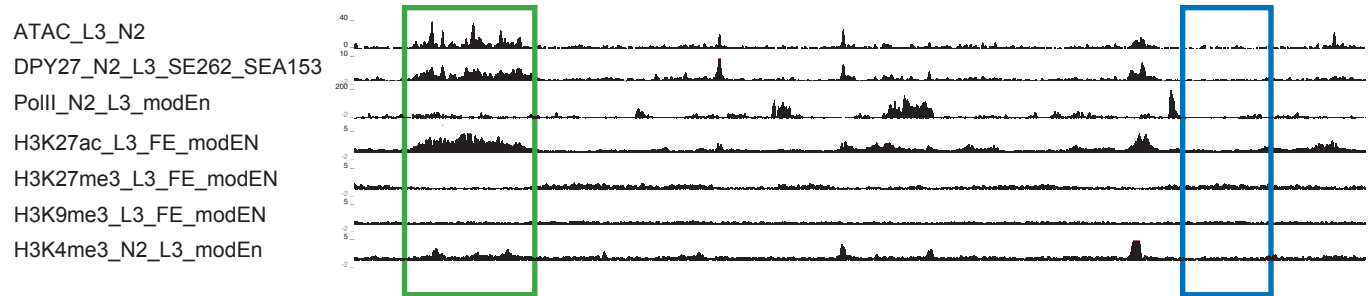
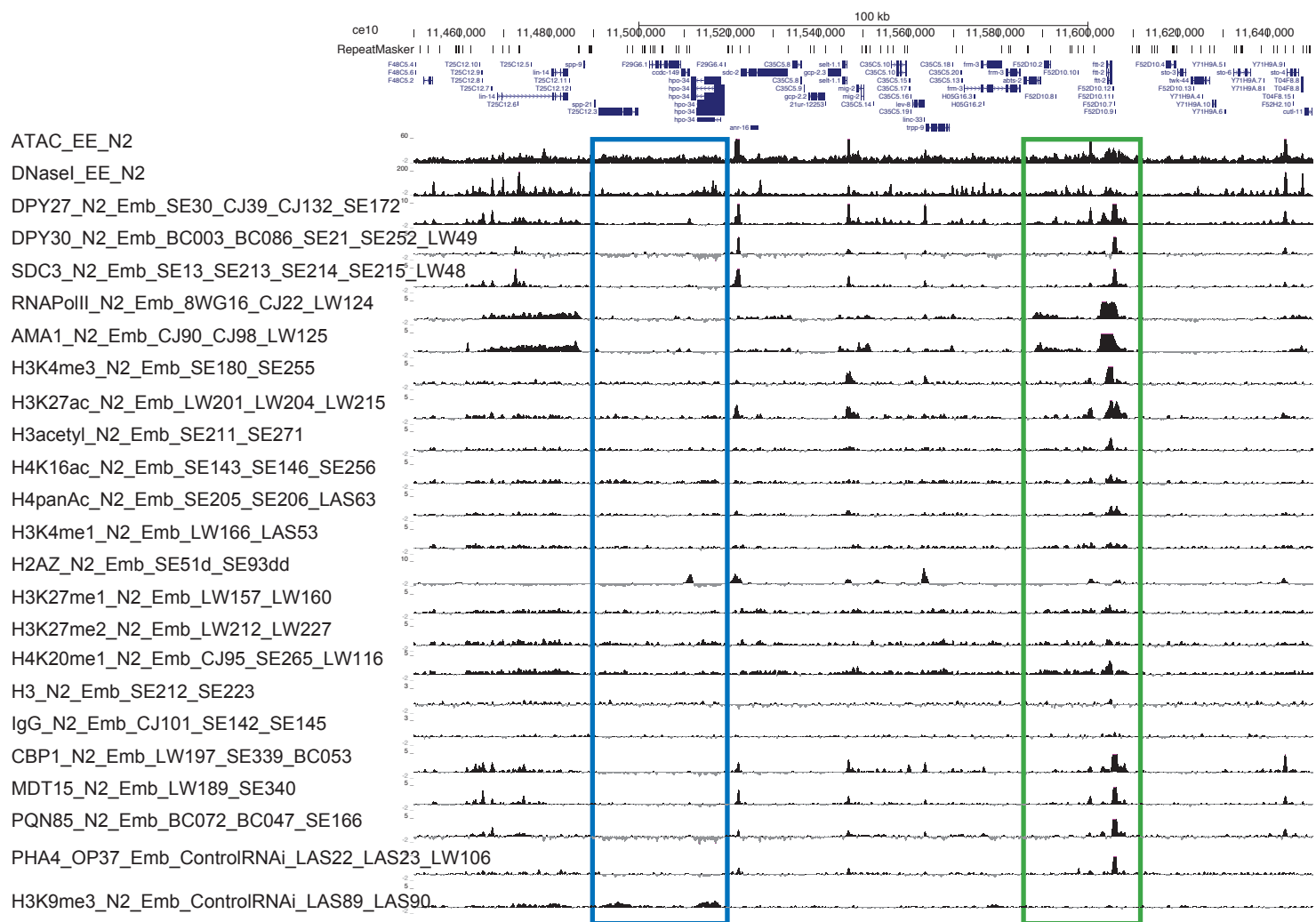
# Supp Fig 1 continued



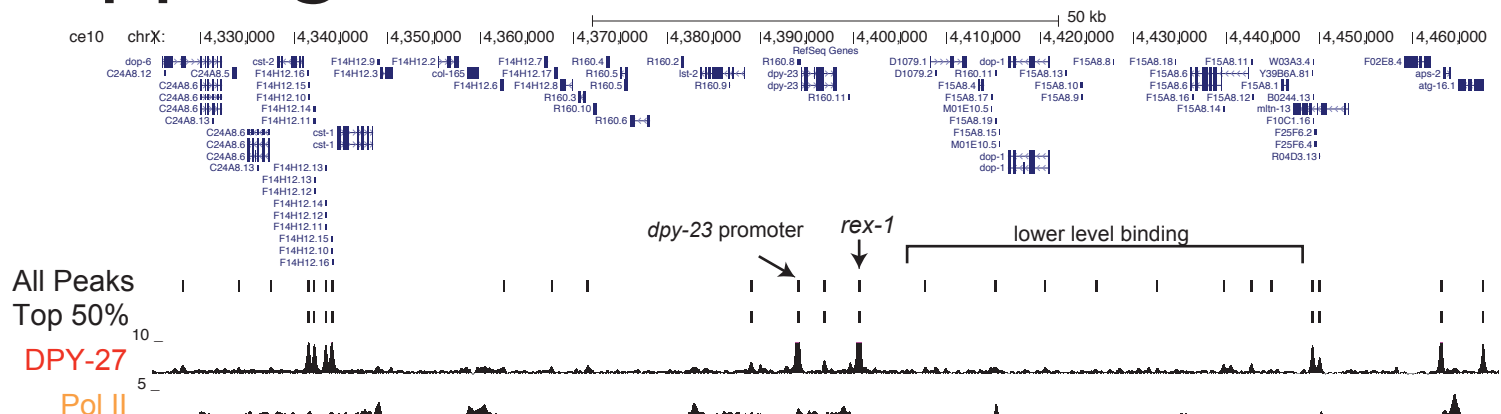
## Supp Fig 1 continued



# Supp Fig 2

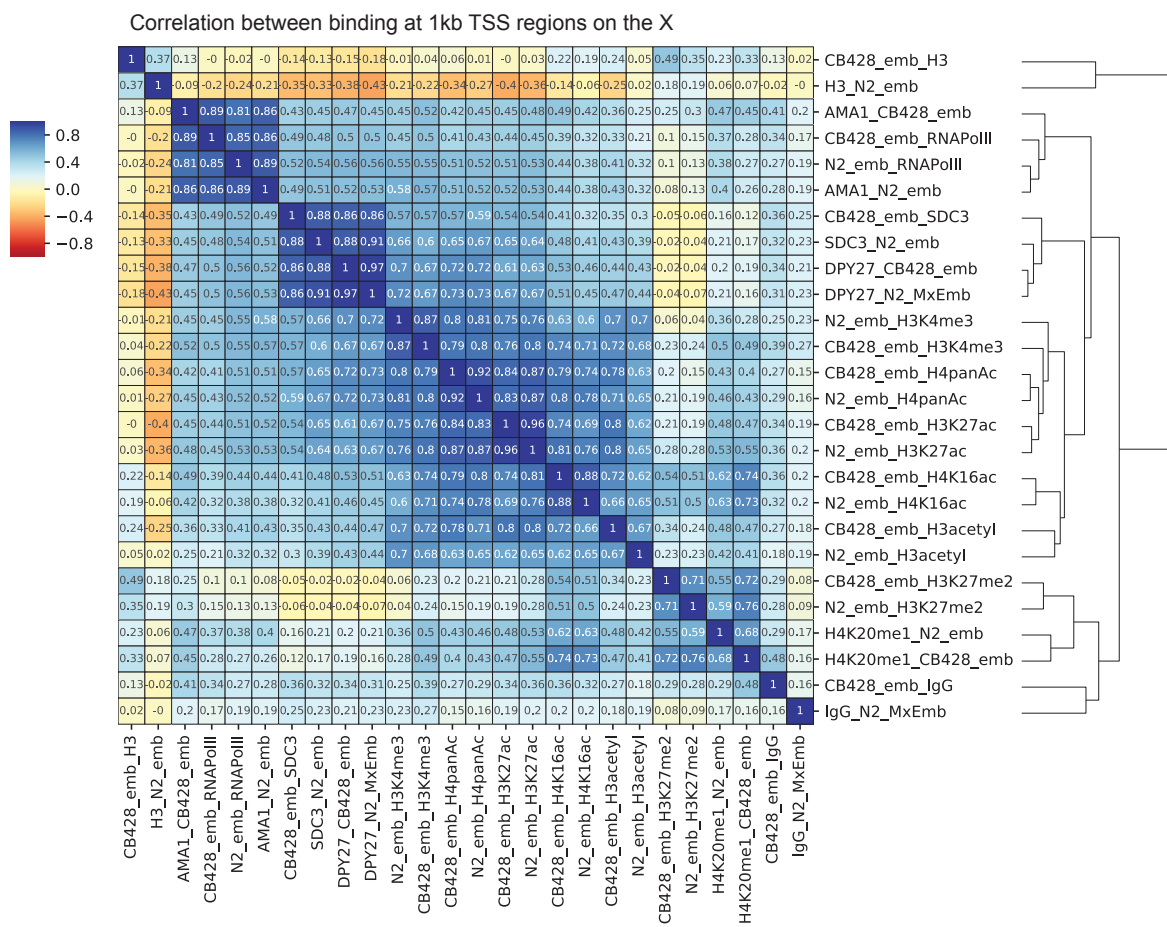


# Supp Fig 3



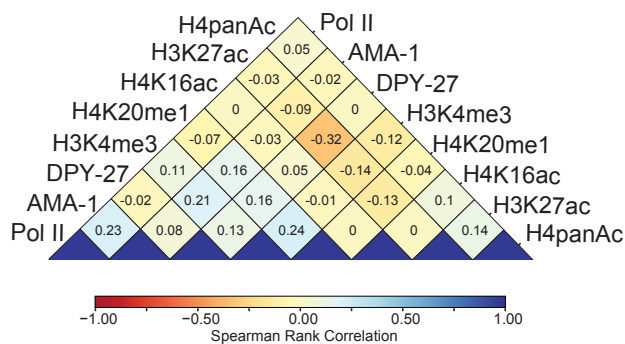
## Supp Fig 4

A

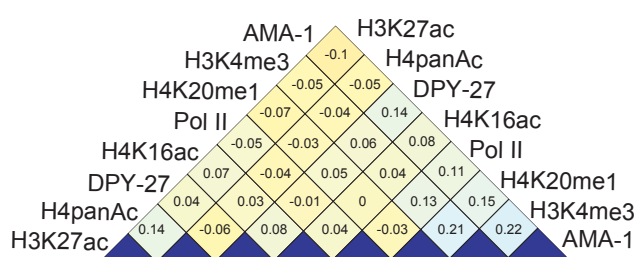


B

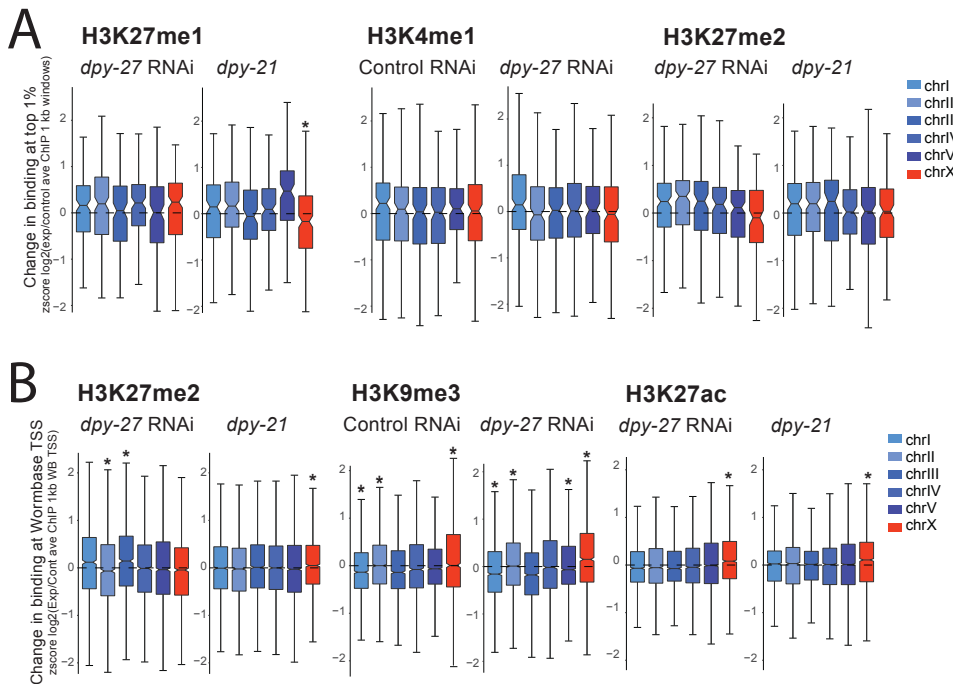
Correlation between change (*dpy-21/wt*) in marks and Pol II binding at 1kb TSS regions on X



Correlation between change (*dpy-21/wt*) in marks and Pol II binding at 1kb TSS regions on autosomes

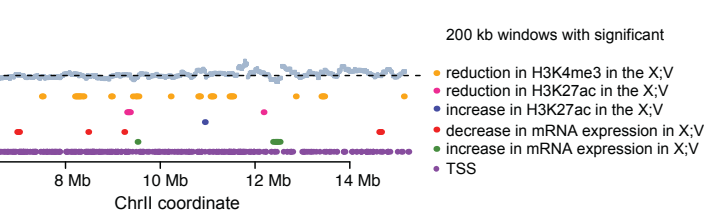
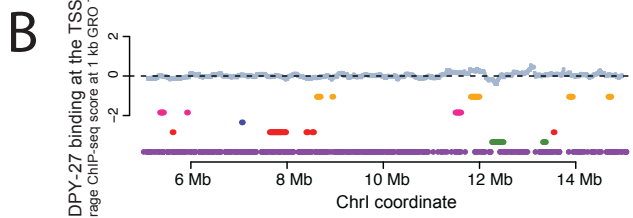
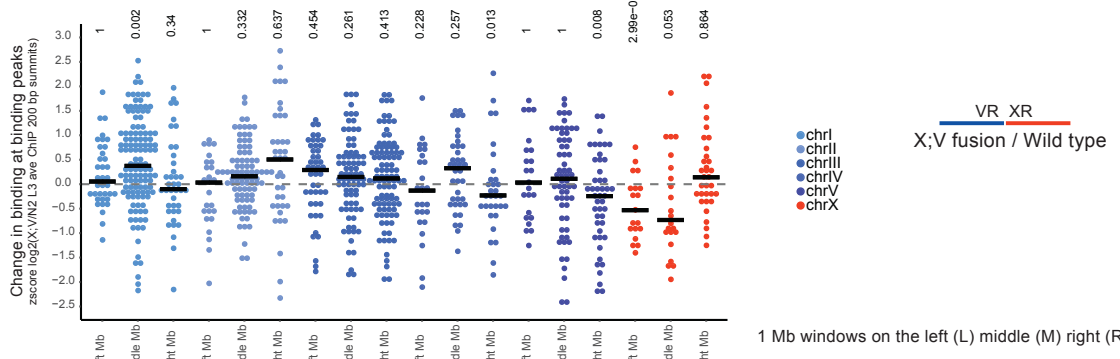


## Supp Fig 5



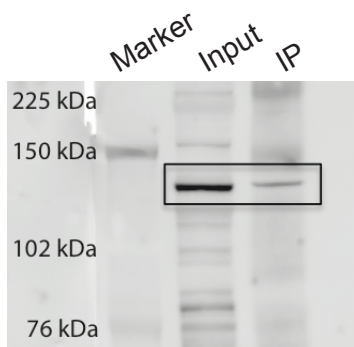
## Supp Fig 6

### A H3K27ac X;V vs wild type at H3K27ac peaks



# Supp Fig 7

## MDT-15 (Q4097)



MDT-15 IP w/ 1 ug SDI-Q4097  
Blotted w/ same 1:2000 dilution  
Expected band size:  
84.5 kDa (isoform A)  
84.2 kDa (isoform B)

